14 Mar 1991, 10:30 am - 12:30 pm

Behavior of Fine Sand Under Cyclic Rotation of Principal Stresses Using the Hollow Cylinder Apparatus

Panos Dakoulas
Rice University, Houston, Texas

Yuanhui Sun
Rice University, Houston, Texas

Proceedings: Second International Conference on Recent Advances in Geotechnical Earthquake Engineering and Soil Dynamics, March 11-15, 1991, St. Louis, Missouri, Paper No. 3.46

Behavior of Fine Sand Under Cyclic Rotation of Principal Stresses Using the Hollow Cylinder Apparatus

Panos Dakoulas
Assistant Professor, Department of Civil Engineering, Rice University, Houston, Texas

Yuanhui Sun
Graduate Student, Department of Civil Engineering, Rice University, Houston, Texas

SYNOPSIS: Results of an experimental investigation on a saturated fine Ottawa Silica Sand subjected to three different types of cyclic tests are presented in this paper. The effects of principal stress rotation at a constant deviator stress on the pore water pressure buildup and the deformation characteristics of sand are evaluated in comparison with results from cyclic triaxial and cyclic torsional simple shear using the hollow cylinder apparatus.

The results presented and discussed in this article, representing a small part of the experimental program, suggest that the effects of rotational shear are more important than the effects of cyclic triaxial loading or cyclic torsional simple shear loading (of the same amplitude) in terms of the rate of pore water pressure buildup, the triggering of a liquefaction flow failure in contractive sand and the rate of accumulation of plastic deformation. Moreover, results from the monotonic test program on fine Ottawa Silica Sand under drained conditions were found in very good agreement with the failure surface incorporated in Lade's constitutive model for frictional materials.

INTRODUCTION

The development of pore water pressures and deformation in saturated sands subjected to cyclic loading has been the subject of several investigations during the last fifteen years. Of particular theoretical and practical interest is the study of the effects of rotation of principal stresses on the pore water pressure buildup and deformation characteristics. Such studies suggest that the deformation characteristics of sands under monotonic and cyclic loading are significantly affected by rotation of principal stresses (Arthur et al, 1980, 1981; Ishihara and Towhata, 1983; Yamada and Ishihara, 1983; Symes et al, 1984, 1988).

Although there is generally agreement that the effects of principal stress rotation are significant and should be taken into account in modeling of soil behavior, the experimental procedures for such testing are by no means conventional. Instead, they are complicated and costly. Thus, usually there are only limited sets of data for the development of constitutive models capable of predicting such unconventional stress paths. The need to clarify our understanding of the phenomena during principal stress rotation was emphasized at the workshop on "Generalized Stress-Strain and Plasticity Theories for Soils" held in Montreal, Canada, in 1980. In this workshop, the participants were provided with experimental data from conventional tests and were asked to make "class A" predictions of new data, including circular rotation of principal stresses. After evaluating a number of widely known plasticity models, Poorooshasb and Selig (1980) concluded that "a comparison of the predictions to test results showed good agreement for simple, monotonic loading stress paths, but *poor agreement for the severe test of the circular stress path*". Some progress has been achieved in understanding these phenomena through experimental investigations since then, but the level of understanding is still far less than desirable. There are also some promising attempts in modeling sand behavior based on the few sets of existing data. Such is a recent study by Wang, Dafalias and Shen (1990), who developed a bounding surface model based on data by Yamada and Ishihara (1983) in order to simulate the sand behavior under rotational shear loading (i.e. a circular rotation of a constant amplitude of the octahedral shear stress) with significant success.

This study concentrates on some aspects of the effects of principal stress rotation during cyclic load. To isolate the effects of rotation from the effects of loading or unloading, it is desirable that, the rotation of principal stresses (σ_1, σ_2, σ_3) occurs at a constant amplitude of the octahedral shear stress τ_{oct} given by

$$\tau_{oct}=\frac{1}{3}\sqrt{(\sigma_1-\sigma_2)^2+(\sigma_2-\sigma_3)^2+(\sigma_3-\sigma_1)^2} \qquad (1)$$

The latter requires the use of an experimental system such as the cubical triaxial apparatus to control properly the magnitudes of σ_1, σ_2, and σ_3 so that τ_{oct} is kept constant. An easier and less expensive alternative solution, is the use of the hollow cylinder apparatus, which can be used to keep constant the deviator stress $\tau_o=(\sigma_1-\sigma_3)/2$. Note that in the latter case, although $\sigma_1-\sigma_3$ remains constant, $\sigma_1-\sigma_2$ and $\sigma_2-\sigma_3$ vary cyclicly during the rotation of principal stresses. However, under certain conditions, the cyclic variation of τ_{oct} may be kept small in amplitude. In the test results presented in this article involving circular rotation of principal stresses using the hollow cylinder apparatus, when $\tau_o=(\sigma_1-\sigma_3)/2$ is kept constant, the oscillation of τ_{oct} is quite small.

In addition to the theoretical interest for understanding the phenomena and for developing constitutive models, there are also some direct applications of the continuous rotation of principal stress directions at a constant deviator stress, such as the cyclic stresses induced by the waves within the sea-bed soil studied by Ishihara and Towhata (1983), as well as (approximately) the cyclic stresses induced by railways or motor vehicles within the underlying soil.

EQUIPMENT FOR HOLLOW CYLINDER TESTING

The experimental program was carried out at Rice University using a newly developed computer-automated experimental system for hollow cylinder testing of soil. The experimental system, which is capable of both stress and strain controlled tests, consists of (see Figure 1):

(a) an axial/torsional servo-hydraulic MTS frame with a 25 kN axial capacity and 250 N.m torque capacity; (b) closed-loop control electronics; (c) a Hewlett-Packard 9000/360 workstation with a maximum speed about 4-5 million instructions per second; (d) a HP-3852A data acquisition and control unit, having a maximum voltmeter speed of 100,000 measurements per second. The system has 24 channels for data acquisition and 2 channels of voltage output for control of the axial and torsional actuators at any desired loading history; (e) pressure control panel and volume change measurement device; (f) a triaxial cell for hollow and solid soil specimens (see Figure 2). The cell has a height of 19 in (48.2 cm) and an inner diameter of 13 in (33.0 cm) and is made of a 1.2 in (3 cm) thick clear cast acrylic cylinder. The load is applied on the soil specimens through a Teflon coated piston having a diameter of 1.5 in (3.8 cm). Calibration tests showed that the friction between the piston and the air bushing is less than 1 per cent for both the axial and torsional directions. The test results are corrected for any piston friction effects.

Figure 1. Experimental System for Hollow Cylinder Testing

TESTED SAND AND SPECIMEN PREPARATION

The sand used in this experimental program is a very fine Ottawa Silica Sand with an mean diameter of D_{50}=0.11 mm, a coefficient of uniformity of C_u=1.66, maximum void ratio e_{max} = 0.95 and minimum void ratio e_{min} =0.57. The specific gravity is G=2.65. The sand mixture was produced by sieving and remixing the commercially available F-125 sand provided by U.S. Silica Company, Ottawa, Illinois. The selected grain size distribution curve is shown in Figure 3. For such a fine sand the effects of membrane penetration are very small and could be neglected.

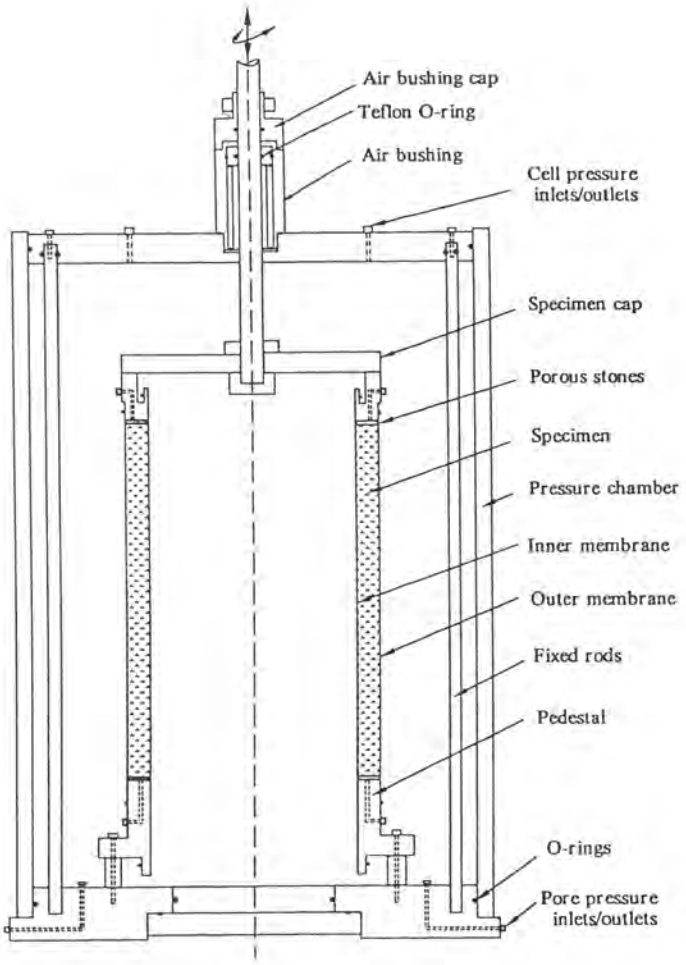

Figure 2.Triaxial Cell for Hollow Cylinder Testing.

Both solid and hollow cylinder specimens were used in this study. The solid specimens have a diameter of 4 in (10.16 cm) and a height of 8 in (20.32 cm), while the hollow cylinder specimens have an inside diameter of 4 in (10.16 cm), outside diameter of 5.5 in (13.97 cm), and height of 8 in (20.32 cm). All specimens were prepared using the moist tamping "undercompaction" technique developed by Ladd (1978). Each specimen was prepared in 15 layers of 6% most sand using varying initial density, so that after compaction, a high degree of uniformity is achieved along the height of the specimen. An initial confining stress of 20 kN/m^2 was applied in the specimen, which was then percolated with CO_2 for one hour and saturated with deaired water. When saturation was complete, the specimen was subjected to a back pressure of 207 kN/m^2 and an effective pressure of 20.7 kN/m^2 for about 12 hours. The specimen was considered to be fully saturated and ready for testing, if the pore pressure response parameter B was at least 0.95. In all performed tests the value of B was larger than 0.96.

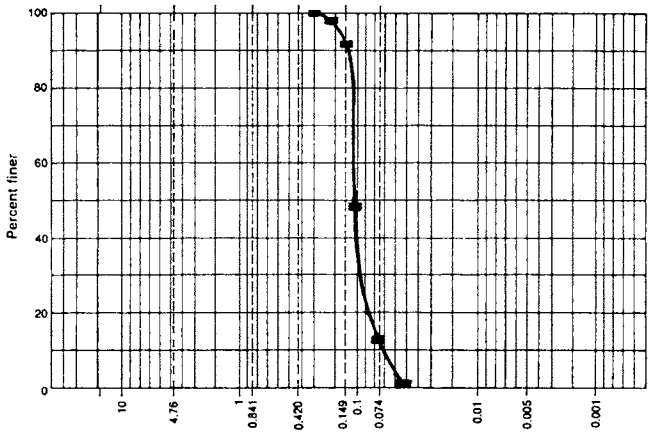

Figure 3. Grain Size Distribution of Fine Ottawa Silica Sand.

EXPERIMENTAL PROGRAM: MONOTONIC TESTS

The entire experimental program includes a series of monotonic and cyclic tests on loose sand of relative density Dr=30% and on dense sand of relative density Dr=75%. Due to space limitations, only small part of the results is presented in this paper, while the rest of the results will be published elsewhere.

Failure Surface of Loose Sand (Dr=30%)

A series of monotonic tests was performed at various stress levels using solid and hollow cylinder specimens in order to establish the failure surface under more general stress conditions, by considering the influence of the intermediate principal stress, σ_2. These tests were performed by consolidating isotropically each specimen from the initial effective confining stress of 20.7 kN/m^2 to the desired level of effective confining stress σ_c'. Then the specimen was sheared by applying axial, torsional or a combination of axial and torsional loads under the condition that the stress point $(\sigma_1', \sigma_2', \sigma_3')$ transversed on the same octahedral plane, i.e. the effective mean stress $p'=(\sigma_1' + \sigma_2' + \sigma_3')/3 = \sigma_c'$ remained constant. This was achieved by applying small changes of the confining pressure, while the axial and torsional loads were automatically adjusted to keep constant p' and the angle β between the major principal stress direction and the vertical direction. This angle is expressed by

$$\tan 2\beta = \frac{2\tau_{vh}}{\sigma_v - \sigma_h} \qquad (2)$$

as shown in Figure 4. For $\beta=0°$, the test is a triaxial compression test with constant p', for $\beta=90°$ the test is a triaxial extension test with constant p', while for $\beta=45°$ the test becomes a torsional simple shear test. The principal stresses are computed by

$$\sigma_1 = \frac{\sigma_v+\sigma_h}{2} + \sqrt{\left(\frac{\sigma_v-\sigma_h}{2}\right)^2 + \tau_{vh}^2} \qquad (3a)$$

$$\sigma_2 = \sigma_h \qquad (3b)$$

$$\sigma_1 = \frac{\sigma_v+\sigma_h}{2} - \sqrt{\left(\frac{\sigma_v-\sigma_h}{2}\right)^2 + \tau_{vh}^2} \qquad (3c)$$

where σ_v and σ_h are the vertical and horizontal (radial and cicumferential) normal stresses, and τ_{vh} is the torsional shear stress.

Figure 4 plots failure points on the octahedral plane with an effective mean p'= 300 kN/m^2. The open circles correspond to the test results, while the solid curve represents the failure surface according to Lade's model for frictional materials (1978, 1990). The failure surface in Lade's model is shaped as an asymmetric bullet with a pointed apex at the origin of the stress axes and is expressed by

$$\left(\frac{I_1^3}{I_3} - 27\right)\left(\frac{I_1}{p_a}\right)^m = \eta_1 \qquad (4)$$

where $I_1 = \sigma_1' + \sigma_2' + \sigma_3'$,

$I_3 = \sigma_1' \sigma_2' \sigma_3'$,

p_a = the atmospheric pressure

and

m and η_1 are material constants.

For the data in Figure 4, m=0 and η_1=12.48. Notice that Lade's model is in very good agreement with the experimental data.

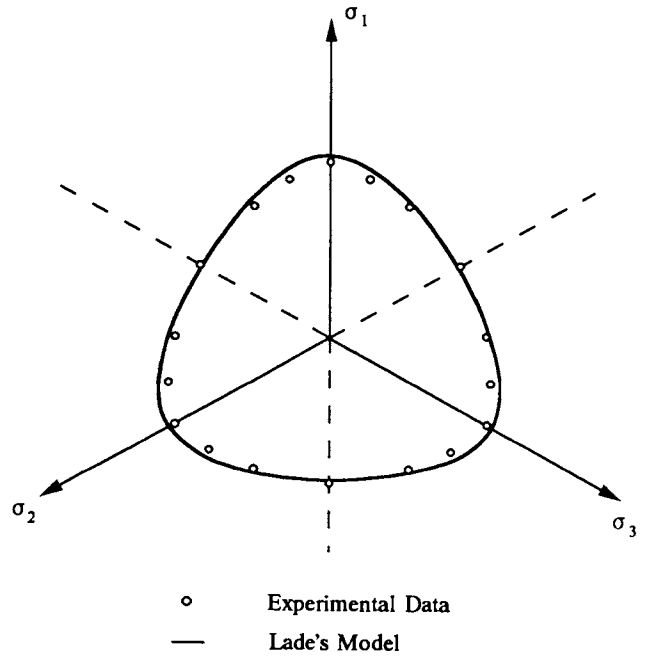

Figure 4. Fine Ottawa Silica Sand: Comparison of Experimental Failure Data on the Octahedral Plane (p'= 300 kN/m^2) with Lade's Model Failure Surface.

CYCLIC TESTS

Results from three different types of cyclic tests are presented and discussed in this article. The performed tests are: (a) a cyclic axial test performed on a solid specimen (b) a cyclic torsional simple shear test performed on a hollow cylinder specimen and (c) a circular rotation of principal stresses with constant deviator stress $\sigma_1 - \sigma_3$, performed on a hollow cylinder specimen. The specimen preparation techniques and the initial density and stress state are identical in all three tests. Note that although test (a) was performed for convenience on solid specimen, while (b) and (c) on hollow cylinder specimens, comparison of monotonic tests results from solid and hollow specimens showed excellent agreement.

All specimens were initially isotropically consolidated to a confining stress $\sigma_c' = p' = 300$ kN/m^2, where they had the same void ratio equal to e=0.819.

Test (a) was performed in undrained conditions by applying a sinusoidal vertical stress resulting into a sinusoidal shear stress of amplitude $\tau_o = (\sigma_v - \sigma_h)/2 = 45$ kN/m^2. Figure 6a depicts the change of axially imposed shear stress and the sudden 90° rotation of principal stresses σ_1 and σ_3 whenever the stress point reaches the origin ($\sigma_1' = \sigma_3' = \sigma_c'$).

Test (b) was performed in undrained conditions by applying a sinusoidal torsional shear stress τ_{hv} of the same amplitude with the shear stress in test (a), i.e. $\tau_{hv} = \tau_o = 45$ kN/m^2. Figure 6b shows the sudden 90° rotation of principal stresses σ_1 and σ_3, whenever the stress point reaches the origin (i.e., $\tau_{hv} = 0$ and $\sigma_1' = \sigma_3' = \sigma_c'$).

Test (c) was performed by applying initially a shear stress of amplitude $\tau_o = (\sigma_v - \sigma_h)/2 = 45$ kN/m^2 under drained conditions, leading to a change of void ratio from e=0.819 to e=0.809 for this specimen. Then, the valves of the pore water were closed and a circular rotation of the shear stress τ_o was performed (at constant amplitude), by using a combination of cyclic vertical shear stress

$$(\sigma_v - \sigma_h)/2 \cos(2\pi f t) = \tau_o \cos(2\pi f t) \qquad (5)$$

and cyclic torsional shear stress

$$\tau_{hv} \sin(2\pi f t) = \tau_o \sin(2\pi f t) \qquad (6)$$

resulting to a constant amplitude total shear stress of

$$\frac{\sigma_1 - \sigma_3}{2} = \sqrt{\left(\frac{\sigma_v - \sigma_h}{2}\right)^2 + \tau_{vh}^2} = \tau_o = 45 \text{ kN/m}^2 \qquad (7)$$

where f is the frequency of cyclic loading, being equal to f=0.1 Hz for all three cyclic tests. Figure 6c shows the circular rotation of the constant amplitude shear stress τ_o and the continuous change of the angle β from 0 to 180°.

RESULTS AND DISCUSSION

Figures 5a and 5b plot the void ratio versus the effective mean stress p' and the shear stress $(\sigma_1 - \sigma_3)/2$, respectively, at the steady of deformation (Poulos, 1981) for the tested sand. The three results at the right of the two plots were obtained from independent monotonic tests, while the three data points on the left correspond to the three cyclic tests. Note that, with . void ratios e=0.809 and 0.819 and $p' = 300$ kN/m^2, the initial consolidation states (e-p') in Figure 5a of the cyclic tests lie in the upper right side of the steady state line (SSL). Moreover, the amplitude of the imposed shear stress $\tau_o = 45$ kN/m^2 is larger than the undrained shear strength at the steady state of deformation. In other words, the three specimens are contractive, and, therefore, the accumulation of excess pore water pressure could lead to either a liquefaction flow failure or at least to a limited flow failure (Mohamad and Dobry, 1986).

Figure 7 plots the effective stress path q-p' for the three tests, while Figures 8 and 9 plot the shear stress, q, and the pore water pressure, u, versus the octahedral strain γ_{oct}, respectively, where γ_{oct} for the case of the hollow cylinder is given by

$$\gamma_{oct} = \frac{2}{3}\sqrt{(\varepsilon_v - \varepsilon_r)^2 + (\varepsilon_r - \varepsilon_h)^2 + (\varepsilon_h - \varepsilon_v)^2 + \frac{2}{3}\gamma_{vh}^2} \qquad (8)$$

in which ε_v, ε_h, ε_r are the normal strains in the vertical, horizontal (circumferential) and radial directions, and γ_{vh} is the shear strain from torsion.

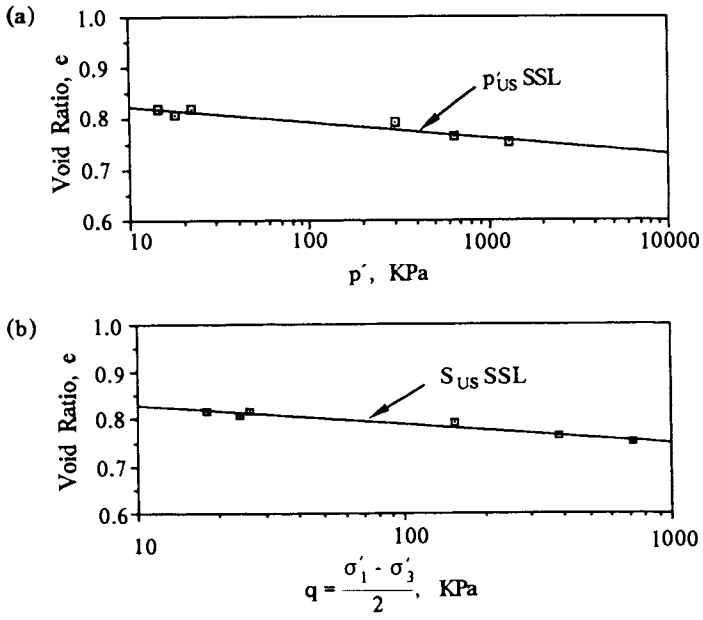

Figure 5. Steady State of Deformation of Fine Ottawa Silica Sand: (a) Void Ratio versus Mean Effective Stress; (b) Void Ratio versus Shear Strength.

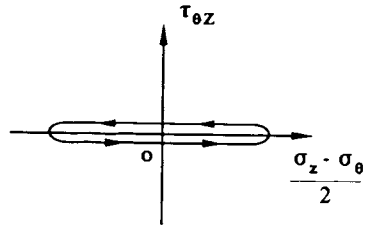

(a) Cyclic Triaxial Shear Test

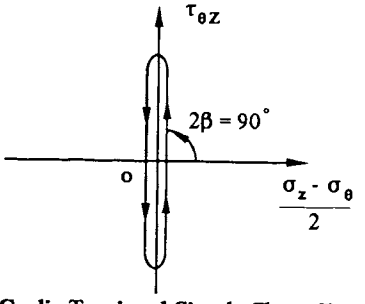

(b) Cyclic Torsional Simple Shear Test

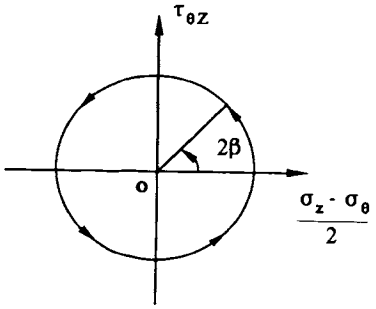

(c) Circular Rotation of Principal Stresses

Figure 6. Orientation and Amplitude of the Shear Stress $\tau_o=(\sigma_1-\sigma_3)/2$ for the Three Cyclic Tests (After Ishihara and Towhata, 1983)

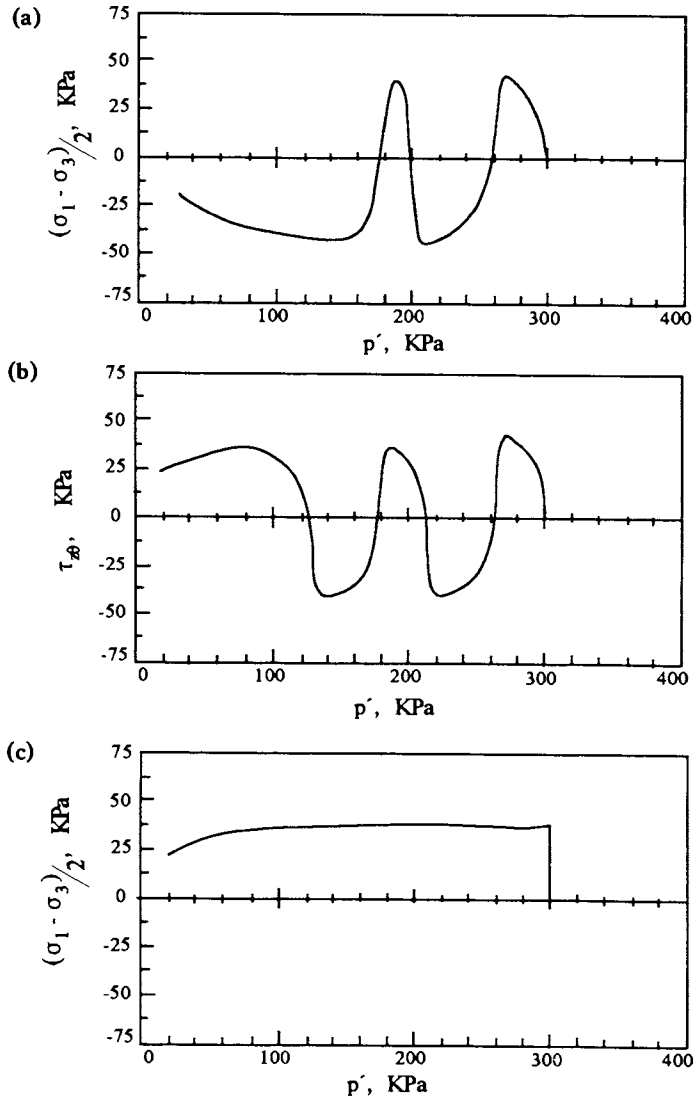

Figure 7. Effective Stress Paths during (a) Cyclic Triaxial Test; (b) Cyclic Torsional Simple Shear Test; and (c) Circular Rotation of Principal Stresses under Constant Deviator Stress.

The most important conclusion derived by comparison of the results in Figures 7a , 7b and 7c, is that cyclic rotation of principal stresses with a constant deviator stress $\sigma_1-\sigma_3$ may induce excess water pressures, which appear to be more significant than those developed in the cyclic axial and torsional simple shear tests. For the presented test results, the pore pressure buildup in the test (c) occurs at a faster rate than for the other two tests. In all three tests the development of excess pore pressure led to a liquefaction flow failure, which occurred in about 1.5 cycles for the cyclic axial test, 2.25 cycles for the cyclic torsional simple shear test, and 0.75 of a rotation of a constant shear stress amplitude $\tau_o=(\sigma_1-\sigma_3)/2$. (Note that, although the application of cyclic load continued after the occurrence of the liquefaction flow failure, for clarity, the presented results end at the steady state of deformation, which can be easily defined from the significant deformation occurring at constant stresses during the sudden liquefaction flow failure.)

The above conclusion is in complete agreement with results from a similar study by Ishihara and Towhata (1983). In this study, Ishihara and Towhata performed the same three

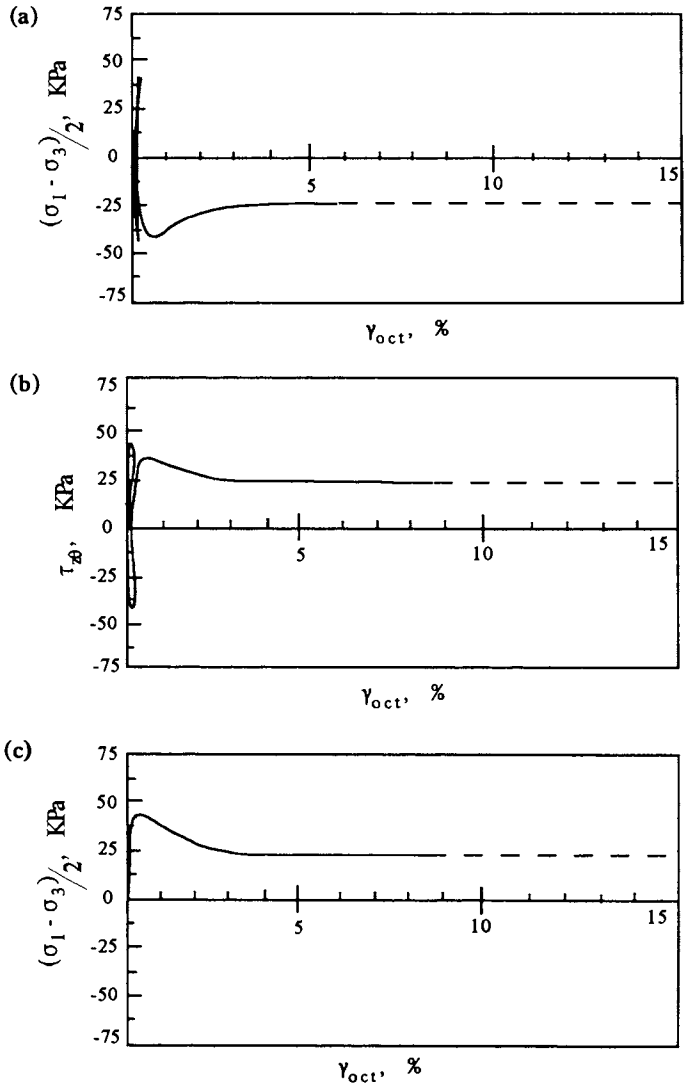

Figure 8. Stress-Strain Curve for (a) Cyclic Triaxial Test; (b) Cyclic Torsional Simple Shear Test; and (c) Circular Rotation of Principal Stresses under Constant Deviator Stress.

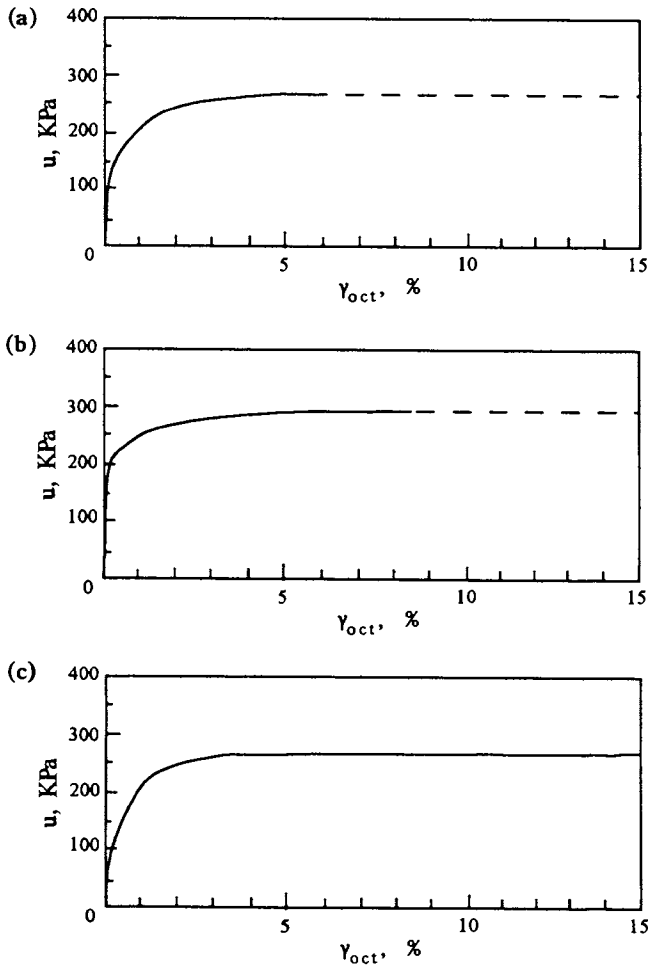

Figure 9. Pore Water Pressure Buildup during (a) Cyclic Triaxial Test; (b) Cyclic Torsional Simple Shear Test; and (c) Circular Rotation of Principal Stresses under Constant Deviator Stress.

types of tests on Toyoura sand with D_{50} = 0.17 mm and a coefficient of uniformity C_u = 2 consolidated at 294 kN/m^2 at a void ratios e=0.800 for the cyclic triaxial, e=0.784 for the torsional simple shear, and e=0.811 for the test with the circular rotation of the principal stress. For an amplitude of cyclic stress equal to $\tau_o=(\sigma_1-\sigma_3)/2=55.5$ kN/m^2, the corresponding numbers of cycles sufficient to cause liquefaction were 6 for test (a), 38 for test (b) and 2 for test (c). Although these numbers of cycles or rotations of τ_o are higher than those in the present study, the trends are consistent for the two sands. (The significantly higher number of cycles for the case of the torsional simple shear test was attributed by Ishihara and Towhata, partly to the smaller value of void ratio of this specimen.)

Of special interest is that the amount of pore water pressure buildup during the first quarter of a cycle (compression loading) is the same for both the axial and torsional simple shear test (Δu=27 kN/m^2). Perhaps surprisingly, the pore pressure during the first quarter of the test involving rotation of principal stresses with a constant shear stress $\tau_o=(\sigma_1-\sigma_3)/2=45$ kN/m^2 shown in Figure 7c, induces the

same amount of pore pressure buildup (i.e. $\Delta u=27$ kN/m^2). A comparison with the results by Ishihara and Towhata shows for the three tests, respectively, $\Delta u=28$ kN/m^2, $\Delta u=22$ kN/m^2 and $\Delta u=25$ kN/m^2, but some of the differences in Δu may by attributed to changes in the initial void ratio in the three specimens.

Notice also that the pore pressure development in the cyclic axial test is more pronounced during extension loading than during compression loading. Indeed, during the first cycle the extension loading induced a pore pressure $\Delta u=52$ kN/m^2, i.e. 92% larger than the pore pressure developed during the compression loading, as shown in q-p´ plot in Figure 7a. This is also observed in the case of the torsional simple shear test in Figure 7b, where the part of simple shear which approaches more the extension loading produces $\Delta u=42$ kN/m^2 (about 55% larger pore pressure increment than the Δu occurring during the opposite loading, approaching towards the compression loading). Similar findings, regarding the difference between compression and extension loading, have been also reported by Ishihara and Towhata (1983), Yamada and Ishihara (1983), Mohamad and Dobry (1986), etc. The corresponding unloadings from the compression and extension during the first cycle yield for both tests (a) and (b) a pore pressure increment $\Delta u=8$ kN/m^2.

If one considers the rotation of the constant shear stress $\tau_o=(\sigma_1-\sigma_3)/2=45$ kN/m^2 as a superposition of a cyclic triaxial shear stress and a cyclic torsional shear stress, the pore pressure buildup must be the combined effect of a simultaneous application of the two cyclic waves. In practice, this is of little significance because the pore pressure buildup is not a linear phenomenon and therefore it is not possible to predict the results of test (c) from the results of tests (a) and (b). Probably due to the mainly elastic response of the sand during the first and second quarter of the first cycle or simply by coincidence, the pore pressure increment during the second quarter of the first rotation of τ_o is $\Delta u=60$ kN/m^2 which is equal to the sum of $\Delta u=52$ kN/m^2 from extension loading of test (a) and $\Delta u=8$ kN/m^2 from shear unloading of test (b). However during the third quarter of the rotation, the induced Δu is 79 kN/m^2 which is much higher than the sum of the extension unloading with $\Delta u=8$ kN/m^2 and the loading in test (b) with $\Delta u=42$ kN/m^2. This may be attributed to the faster rate of accumulation of the excess water pressure in test (c) resulting in a faster rate of yielding and ultimately in an earlier liquefaction flow failure.

With respect to the strains developed in each of the three tests during the first cycle of loading (not shown in Figure 8 due to the improper scale of the octahedral strain), it was found that during the first quarter of the cycle, test (a) induced $\gamma_{oct}=0.065\%$ (almost all of which is elastic strain), test (b) induced $\gamma_{oct}=0.110\%$ (of which 0.085% is elastic and 0.025% is plastic strain) and test (c) induced $\gamma_{oct}=0.220\%$ (of which 0.150% is elastic and 0.070% is plastic strain). Again, the rate of plastic deformation is faster during the rotation of a constant deviator stress than during the cyclic triaxial or cyclic simple shear tests of the same amplitude. The difference becomes even more pronounced during the third quarter of the first cycle, where test (a) induced a change of $\gamma_{oct}=0.125\%$ (of which 0.060% is elastic and 0.065% is plastic), test (b) induced a change $\gamma_{oct}=0.190\%$ (of which 0.100% is elastic and 0.090% is plastic strain) and test (c) induced a change of $\gamma_{oct}=0.658\%$ at which strain the sand reached the "phase of transformation" and a liquefaction flow failure was triggered.

Note that the above findings are preliminary and based on the evaluation of a limited set of data. More tests were performed using different amplitudes of cyclic load and different types of stress paths. A more detailed analysis and assessment of all obtained results will soon follow and be published elsewhere.

CONCLUSIONS

From the experimental study described above, the following conclusions may be drawn:

1. The experimental results presented here confirm previous findings that the circular rotation of a constant amplitude deviator stress $\sigma_1-\sigma_3$ has a significant effect on the development of excess pore water pressures and deformation characteristics of saturated sands.

2. The results showed that the rate of excess pore water pressure buildup is faster during the rotation of a constant amplitude deviator stress than during a cyclic triaxial test or a torsional simple shear test of the same amplitude.

3. The rate of accumulation of plastic deformation is faster in the rotational shear test than in the other two cyclic tests.

4. Also, the number of cycles to trigger a liquefaction flow failure in contractive saturated sand is smaller during a rotational shear test than during the other two cyclic tests.

5. The failure criterion provided by Lade's constitutive model for frictional materials is in very good agreement with the experimental data obtained for the loose fine Ottawa Silica Sand used in this study.

ACKNOWLEDGEMENTS

This work is part of a research effort to develop experimental data for constitutive modeling of soil, supported by the National Science Foundation under the grant number MSM-880975. This support is gratefully acknowledged. The authors wish to thank also Mr. Shinyuan Yu for his help during the experimental program.

REFERENCES

Arthur, J., Chua, K., Dunstan, T. and Rodriguez, J. (1980), "Principal Stress Rotation: A Missing Parameter", Journal of Geotechnical Engineering, ASCE, Vol.106, GT4, pp. 419-433.

Arhur, J., Beckenstein, S., Germaine, J. and Ladd, C. (1981), "Stress Path Tests with Controlled Rotation of Principal Stress Directions", Laboratory Shear Strength of Soil, ASTM STP 740, Eds. Yong, R. and Towsend, F., pp. 516-540.

Dobry, R. et al., (1982), "Prediction of Pore Water Pressure Buildup and Liquefaction of Sands During Earthquakes by the Cyclic Strain Method", National Bureau of Standards, Building Science Series 138, U.S. Dept. of Commerce.

Ishihara, K., and Towhata. (1983), "Sand Response to Cyclic Rotation of Principal Stress Directions as Induced by Wave Loads", Soils and Foundations, Vol. 23, No. 4.

Ladd, R. (1978), "Preparing Test Specimens Using Undercompaction", Geotechnical Testing Journal, GTJODJ, Vol. 1, No. 1, pp. 16-23.

Lade, P. and Kim, M. (1988), "Single Hardening Constitutive model for Frictional materials III. Comparisons with Experimental Data", Computers and Geotechnics, Vol. 6, pp. 31-47.

Lade, P. (1990), "Single Hardening Model with Application to NC Clay", Journal of Geotechnical Engineering, ASCE, Vol.116, No. 3, pp. 394-414.

Mohamad, R. and Dobry, R. (1986), "Undrained Monotonic and Cyclic Triaxial Strength of Sand, Journal of Geotechnical Engineering, ASCE, Vol.112, No. 10, pp. 941-958.

Poorooshasb, H. B. and Selig, E. T. (1981), Group 2 report on "Workshop on Plasticity Theories and Generalized Stress-Strain Modelling of Soil, Proc. of a workshop on Plasticity and Generalized Stress-Strain in Geotechnical Engineering, Editors, Yong, R. and Ko, H., ASCE, pp.102-131.

Poulos, S. (1981), "The Steady State of Deformation", Journal of Geotechnical Engineering, ASCE, Vol. 107, pp. 553-562.

Symes, M., Gens, A. and Height, D. (1984), "Undrained Anisotropy and Principal Stress Rotation in Saturated Sand", Geotechnique, Vol. 34, No.1, pp. 11-27.

Symes, M., Gens, A. and Height, D. (1988), "Drained Principal Stress Rotation in Saturated Sand", Geotechnique, Vol. 38, No.1, pp. 59-81.

Sun, Y. and Dakoulas, P. (1990), "Experimental Investigation and Constitutive Modeling of Cohesionless Soil", Rice Report to National Science Foundation, Rice University, Houston, Texas.

Tatsuoka, F., Muramata, M., and Sasaki, T. (1982), "Cyclic Undrained Stress-Strain Behavior of Dense Sands by Torsional Simple Shear Test", Soils and Foundations, Vol. 22, No. 2, pp. 55-69.

Yamada, Y., and Ishihara, K. (1983), "Undrained Deformation Characteristics of Sand in Multi-Directional Shear", Soils and Foundations, Vol. 23, No. 1.

Wang, Z., Dafalias, Y., and Shen, C. (1990), "Bounding Surface Hypoplasticity Model for Sand", Journal of Engineering Mechanics, ASCE, Vol. 116, No. 5, pp.983-1001.